

On the Estimation of Lagrangian Diffusivity: Influence of Nonstationary Mean Flow

YU-KUN QIAN AND SHIQU PENG

*State Key Laboratory of Tropical Oceanography, South China Sea Institute of Oceanology,
Chinese Academy of Sciences, Guangzhou, China*

CHANG-XIA LIANG

South China Sea Marine Prediction Center, State Oceanic Administration, Guangzhou, China

RICK LUMPKIN

NOAA/Atlantic Oceanographic and Meteorological Laboratory, Miami, Florida

(Manuscript received 21 March 2014, in final form 22 July 2014)

ABSTRACT

Eddy-mean flow decomposition is crucial to the estimation of Lagrangian diffusivity based on drifter data. Previous studies have shown that inhomogeneous mean flow induces shear dispersion that increases the estimated diffusivity with time. In the present study, the influences of nonstationary mean flows on the estimation of Lagrangian diffusivity, especially the asymptotic behavior, are investigated using a first-order stochastic model, with both idealized and satellite-based oceanic mean flows. Results from both experiments show that, in addition to inhomogeneity, nonstationarity of mean flows that contain slowly varying signals, such as a seasonal cycle, also cause large biases in the estimates of diffusivity within a time lag of 2 months if a traditional binning method is used. Therefore, when assessing Lagrangian diffusivity over regions where a seasonal cycle is significant [e.g., the Indian Ocean (IO) dominated by monsoon winds], inhomogeneity and nonstationarity of the mean flow should be simultaneously taken into account in eddy-mean flow decomposition. A temporally and spatially continuous fit through the Gauss–Markov (GM) estimator turns out to be very efficient in isolating the effects of inhomogeneity and nonstationarity of the mean flow, resulting in estimates that are closest to the true diffusivity, especially in regions where strong seasonal cycles exist such as the eastern coast of Somalia and the equatorial IO.

1. Introduction

Phenomena associated with the spreading of passive tracers in the ocean, such as plankton, marine debris, and chemical pollutants (e.g., oil), are of practical importance. These problems are usually described by an advection–diffusion model, in which a diffusivity coefficient is employed. Finding a proper diffusivity coefficient for the advection–diffusion model is the pursuit of many studies since the magnitude of diffusivity and how it varies in space and time still remain unclear.

Theoretical studies have tried to seek mathematical expressions of diffusivity. Under the assumptions of a homogeneous and stationary eddy field, Taylor (1922) related the diffusivity to the product of eddy velocity variance and Lagrangian integral time scale. Davis (1987, 1991) regarded the diffusivity as an observable quantity and generalized the diffusivity into a second-order tensor to describe quasi-2D diffusion in an inhomogeneous eddy field. These methods are categorized as single-particle statistics (LaCasce 2008) that require only a large number of current-following (Lagrangian) observations from oceans. The increasing Lagrangian observations by satellite-tracked subsurface floats and surface drifters have facilitated researches on the estimates of diffusivity over various ocean basins (LaCasce 2008; Lumpkin and Pazos 2007).

One important assumption upon which those diffusion theories are based is the scale-separation assumption. However, this assumption is not satisfied because

Corresponding author address: Shiqiu Peng, State Key Laboratory of Tropical Oceanography, South China Sea Institute of Oceanology, Chinese Academy of Sciences, West Xiangang Road No. 164, Guangzhou, China.
E-mail: speng@scsio.ac.cn

no spectral gap between the large- and small-scale motions is found in the real ocean. Fortunately, Davis's (1991) theory relaxes this hypothesis by introducing a "history term" that allows interaction between large- and small-scale motions, and the scale-separation assumption could thus be made for practical purposes. In this assumption, velocity \mathbf{u} can be separated into a large-scale background mean flow \mathbf{U} that is usually well captured by numerical models and a small-scale (subgrid scale) eddy/residual velocity $\mathbf{u}' = \mathbf{u} - \mathbf{U}$ that cannot be resolved by models (especially coarse-resolution climate models). Estimation of eddy diffusivity is based on \mathbf{u}' and the scale separation would thus affect the accuracy of the estimates. In the real ocean, both the mean and eddy fields can be inhomogeneous and nonstationary. Therefore, the calculation procedures of diffusivity based on these theories should be elaborated so that they can be applied to complex oceanic flows. Here, the effects of inhomogeneity and nonstationarity of \mathbf{U} on diffusivity estimation are summarized.

Inhomogeneity of the mean flow implies that $\mathbf{U}(\mathbf{x})$ varies with space \mathbf{x} . Studies (e.g., Davis 1991; Taylor 1953) have demonstrated that the spatial gradient of $\mathbf{U}(\mathbf{x})$ would contribute to the particle dispersion [known as shear dispersion, see review by Young and Jones (1991)] and lead to an increase of estimated diffusivity with time lags (e.g., Bauer et al. 1998; Oh et al. 2000). Therefore, inhomogeneity of $\mathbf{U}(\mathbf{x})$ should be taken into account in the scale separation. A common way to reduce the shear dispersion is using a binning technique. This approach groups Lagrangian observations into geographic bins, and \mathbf{U} is estimated as the average of all observations within each bin. Thus, $\mathbf{U}(\mathbf{x})$ varies as a function of bin but remains constant inside a bin. The common rectangular bin has also been modified, for example, into overlapping circular bins (e.g., Poulain 2001; Poulain and Zambianchi 2007) that allow for smooth estimation of $\mathbf{U}(\mathbf{x})$ or elliptic bins (e.g., Johnson 2001; Lumpkin and Johnson 2013) that are oriented following variance ellipses. However, shear dispersion still exists within bins if bin size is not small enough to resolve strong shear flows such as western boundary currents or jets. Reducing the bin size could give a better resolution of $\mathbf{U}(\mathbf{x})$, but on the other hand would reduce the samples within bins, leading to a statistical result of low significance and a $\mathbf{U}(\mathbf{x})$ field potentially dominated by noise. Besides, smaller bins also make the stationarity assumption dubious (e.g., bins over the Gulf Stream meanders). Bauer et al. (1998) proposed an optimized bicubic spline to fit $\mathbf{U}(\mathbf{x})$. Compared to the binning technique, their spline method has the advantage that the estimated $\mathbf{U}(\mathbf{x})$ is a smooth and continuous function of space, allowing for a better resolution of the shear. Then the values of \mathbf{u}' can be computed more accurately

by subtracting the exact values of $\mathbf{U}(\mathbf{x})$ along drifter trajectories, rather than discrete bin-mean values. They provided a concrete example to show that the spline technique tends to make diffusivity converge to an asymptotic value while smaller bin size would only reduce the increasing rate of the estimated diffusivity for larger time lags. Since the spline method is quite efficient in isolating shear dispersion (i.e., the effect of inhomogeneous mean flow), it has been adopted in many studies (e.g., Bauer et al. 2002; Falco et al. 2000; Falco and Zambianchi 2011; Maurizi et al. 2004; Veneziani et al. 2004).

Nonstationarity of the mean flow implies that $\mathbf{U}(t)$ varies as a function of time t . However, this feature has been less well addressed in the literature than spatial inhomogeneity. Davis (1991) suggested that \mathbf{U} should be estimated by taking observations of many years, and ocean variability within this time scale would have an effect on scale separation. Temporal variabilities from seasonal to interannual time scales are obviously within the range of consideration and could be well resolved by numerical models as compared to eddy-scale motions. The seasonal cycle is typically the most dominant signal among these low-frequency variabilities. However, many works do not explicitly take into account seasonal variation of $\mathbf{U}(t)$, which can be justified if the domains of interest do not show strong seasonal variability. This is not true in monsoon-dominated regions such as the tropical Pacific, Atlantic, and Indian Oceans. An analogous method to deal with nonstationarity is to construct $\mathbf{U}(t)$ in different temporal bins, that is, grouping observations into different seasons and then obtaining \mathbf{u}' with respect to seasonal means. Bauer et al. (2002) grouped drifter observations into four seasons (3 months each) to ensure stationarity within each seasons when estimating the diffusivity in the equatorial Pacific. Maurizi et al. (2004) used only two seasons (6 months each) when analyzing the surface circulation of the Adriatic Sea. Quite recently, Zhurbas et al. (2014) calculated diffusivities in the Indian Ocean relative to a monthly varying mean (1 month each) and found that the estimated diffusivities are smaller than those relative to a constant mean. Their treatment of the nonstationary $\mathbf{U}(t)$ actually extends the binning technique from spatial bins to temporal bins, and within each temporal bin, stationarity is approximately assumed. Problems of the spatial binning technique, however, still exist for temporal bins. Longer (fewer) bins cannot ensure stationarity, while shorter (more) bins cannot guarantee sufficient samples for statistical significance. Approaches capable of continuously estimating the temporal variations (similar to spatial spline method) are desirable for isolating the effect of nonstationary $\mathbf{U}(t)$. Recently, when estimating

the diffusivity over the South China Sea region where monsoon winds dominate, Qian et al. (2013) have found that seasonal variation can be efficiently included in $\mathbf{U}(\mathbf{x})$ by using a Gauss–Markov (GM) estimator proposed by Lumpkin (2003). Asymptotic diffusivities can then be approximately obtained after removing seasonal cycles.

Although Qian et al. (2013) as well as Zhurbas et al. (2014) have shown that seasonal variation would bias the diffusivity if not removed from \mathbf{u}' , it still remains unclear how the nonstationary $\mathbf{U}(t)$ affects the estimation, especially the asymptotic behavior of diffusivity. In addition, whether the seasonal binning method can eliminate the influence of nonstationary $\mathbf{U}(t)$ is not well demonstrated. Recently, Lumpkin and Johnson (2013) improved Lumpkin's (2003) method by adding spatial terms into the GM estimator that could simultaneously estimate multiscale temporal variability and spatial variation of $\mathbf{U}(\mathbf{x}, t)$ within bins, providing a new way for scale separation. This new method, however, has not been fully tested regarding its efficiency in isolating the temporal and spatial variability of $\mathbf{U}(\mathbf{x}, t)$ in the calculation of diffusivity. Therefore, it is best to test the performance of the new GM method in fitting $\mathbf{U}(\mathbf{x}, t)$ and compared it to those of other methods in the framework of idealized mean flows. If this method can well capture the inhomogeneous and nonstationary $\mathbf{U}(\mathbf{x}, t)$, it could be applied to estimate diffusivity over regions such as the Indian Ocean where both inhomogeneity and nonstationarity are significant (e.g., Lumpkin and Johnson 2013; Shenoi et al. 1999).

The rest of paper is organized as follows to address the above issues. Section 2 describes the methods. Results are presented in sections 3 and 4. Conclusions and discussion are given in section 5.

2. Methods

Generating synthetic drifters in idealized or model output flow has been widely used in diffusion-related studies (e.g., De Dominicis et al. 2012; Griesel et al. 2010; Koszalka and LaCasce 2010; McClean et al. 2002; Oh et al. 2000; Veneziani et al. 2005). This method has several obvious advantages. First, the background mean flow $\mathbf{U}(\mathbf{x}, t)$ and Lagrangian parameters (e.g., integral time scale and diffusivity) are already prescribed or determined. Second, synthetic drifter data are free from complex data processing, such as high-frequency filtering to suppress tidal/inertial signals (e.g., Chaigneau and Pizarro 2005; Poulain 2001), wind-slip corrections (e.g., Niiler 2001; Poulain et al. 2009), and drogued/undrogued drifter reassessment (e.g., Grodsky et al. 2011; Lumpkin et al. 2013; Rio 2012). Third, if the computational condition allows, an arbitrarily large number of synthetic

drifter could be deployed to overcome the “array bias” (Davis 1991) as well as seasonal sampling bias.

a. Stochastic model

To simulated synthetic drifters in a prescribed background mean flow, stochastic (random flight/walk) models are usually adopted. Zero-order, first-order, and second-order stochastic models are most commonly used (Griffa 1996; LaCasce 2008), in which displacement, velocity, and acceleration are noised variables, respectively. The simplest zeroth-order model cannot be applied to inhomogeneous turbulent field because it does not meet the “well-mixed” criterion proposed by Thomson (1987). Moreover, it cannot be applied to motions of time scale smaller than the Lagrangian integral velocity time scale, since its autocorrelation function is a delta function (Griffa 1996). The first-order model becomes a little more complex and could resolve finite velocity time scale motion. Although it has an unrealistic delta autocorrelation function of acceleration as compared to that of the second-order model and may also fail the well-mixed criterion, it is sufficient for the present study in which diffusivity is specified constantly and will be used here.

Assuming two components of velocity are independent, the first-order stochastic model can be written in one-dimensional form as (e.g., Maurizi et al. 2004; Risken 1996)

$$du' = -\frac{u'}{T_L} dt + \frac{\sqrt{2\kappa^\infty}}{T_L} dW, \quad \text{and} \quad (1)$$

$$dx = (U + u')dt, \quad (2)$$

where U and u' are the advective background velocity and eddy velocity, x is the displacement, T_L is the Lagrangian integral time scale, κ^∞ is the asymptotic eddy diffusivity, and dW is a random increment following normal distribution $N(0, dt)$ (i.e., a Weiner process of infinitesimal variance). By specifying two constant parameters of κ^∞ and T_L (the eddy field u' becomes homogeneous and stationary), synthetic drifters released in a specified U can be tracked by integrating Eqs. (1) and (2) forward. The corresponding eddy velocity autocovariance is

$$P(\tau) = \frac{\kappa^\infty}{T_L} \exp\left(-\frac{\tau}{T_L}\right), \quad (3)$$

where τ is the time lag. Equation (1) is an Ornstein–Uhlenbeck process. For practical purposes, Eq. (1) should be discretized with a finite time interval Δt so that it becomes a first-order autoregressive model whose autocovariance is different from Eq. (3). However, the difference is negligible when $\Delta t \ll T_L$. This requirement is roughly met by using $\Delta t = 1/4$ days and $T_L = 4$ days

here, and Eq. (3) is thus used as the analytic reference for estimated autocovariance.

b. Estimation of lateral eddy diffusivity

The single-particle diffusivity tensor is defined as (Davis 1991)

$$\kappa_{ij}(\tau) = \int_{-\tau}^0 P_{ij}(t) dt = \int_{-\tau}^0 \langle u'_i(0) u'_j(t) \rangle_L dt, \quad (4)$$

where index i or j stands for the zonal or meridional component, P_{ij} is the component of velocity covariance matrix, and $\langle \cdot \rangle_L$ is the Lagrangian ensemble average over time and space at τ before/after the drifter is located in a domain of interest. The above calculation is done using the pseudotrack method following Swenson and Niiler (1996). Every data point in an area of interest is considered as the initial point of a pseudotrack with both positive and negative values of time lag τ . To obtain the diffusivity that is calculated from u' , the mean flow U

needs to be estimated first. For comparison, three techniques are employed for this: the classical spatial binning technique, the seasonal binning technique (i.e., estimating bin mean for each seasons), and the Gauss–Markov estimator. Once U is obtained by each of the three techniques, u' is computed by subtracting U from u .

c. Gauss–Markov estimator

Drifter data are first grouped into geographical bins, and all velocity observations in each bin are treated as a series consisting of large-scale and eddy-scale motions, that is, $u = U + u'$. The large-scale component U is modeled following the method of Lumpkin and Johnson (2013):

$$U = \mathbf{A}\mathbf{z}, \quad (5)$$

where \mathbf{z} is the amplitude coefficient matrix for temporal and spatial variabilities to be determined in matrix \mathbf{A} . Components of \mathbf{A} are expressed as

$$\mathbf{A}_l = [1 \quad \sin(2\pi t_l) \quad \cos(2\pi t_l) \quad \sin(4\pi t_l) \quad \cos(4\pi t_l) \quad x_l \quad x_l^2 \quad y_l \quad y_l^2 \quad x_l y_l], \quad (6)$$

where the subscript l indicates that observation l is collected at time t_l (in unit of year); x_l and y_l are the zonal and meridional distances from bin center, non-dimensionalized by dividing by 1° longitude and latitude. The first term stands for a constant mean, the next four terms are for the seasonal (annual/semiannual) variability, and the last five terms are for the spatial variability within a bin. Thus, the treatment of U has simultaneously taken into account the inhomogeneity and nonstationarity.

The amplitude coefficient matrix \mathbf{z} can be computed by the GM estimator (Lumpkin and Johnson 2013; Wunsch 1996)

$$\mathbf{z} = \mathbf{R}_z \mathbf{A}^T (\mathbf{A} \mathbf{R}_z \mathbf{A}^T + \mathbf{R}_n)^{-1} u, \quad (7)$$

provided the a priori covariance matrix \mathbf{R}_z of the unknown \mathbf{z} and the variance structure \mathbf{R}_n of the eddy noise u' (details of \mathbf{R}_z and \mathbf{R}_n will be provided later for different tests). The superscript T stands for matrix transpose. After obtaining \mathbf{z} , U is calculated through Eq. (5).

3. Results from idealized scenarios

Idealized tests are carried out first to show the effects of nonstationary $U(t)$ in a clear and illustrative way. A domain (10°S – 10°N , 140° – 200°E) centered on the equator with 301×101 longitude/latitude grids (0.2° grid spacing) is set up. Synthetic drifters are then deployed uniformly in the domain with 0.35° spacing and tracked for 2 yr. This

spacing (0.35°) is a trade-off between computational load and high statistical significance. Thus, at initial time, 4800 drifters in all will be deployed simultaneously and a portion of them may drift or be advected out of the domain. Drifter motion is governed by Eqs. (1) and (2) with $\kappa^\infty = 1 \times 10^7 \text{ cm}^2 \text{ s}^{-1}$ and $T_L = 4$ days. A coarse bin of 2° (as compared to domain grid of 0.2°) is chosen here for the estimation of U . Smaller bins (e.g., 0.5°) will reduce the shear dispersion, and thus we choose 2° bins here to keep some shear effect inside the bin so that it can be clearly identified. Only a subdomain (2°S – 2°N , 168° – 172°E) is considered as the origins of pseudotracks. Four tests (Tests I–IV) are designed (Table 1) with a transition from highly idealized to less idealized oceanic currents.

As a first step of the test, a constant $U = 4 \text{ cm s}^{-1}$ is used (Test I). The mean flow is completely homogeneous and stationary so that the simple binning technique is sufficient to provide an accurate estimate of U . Figure 1 shows the velocity covariance and eddy diffusivity estimated using Eq. (4). Both the estimated zonal and meridional velocity autocovariance (P_{xx} and P_{yy}) nearly overlap with the analytic solution given by Eq. (3). The estimated symmetric diffusivity components (κ_{xx} and κ_{yy}) are also quite close to the analytic solution and asymptote to the specified value of $\kappa^\infty = 1 \times 10^7 \text{ cm}^2 \text{ s}^{-1}$ after 20 days. The asymmetric components (P_{xy} and P_{yx}) are close to zero because the two velocity components are integrated independently and

TABLE 1. Summary of the zonal mean advective flow in four idealized tests (Test I–IV). The mean flow is the sum of a constant mean flow, harmonic oscillations, and a mean flow shear. The variables A , T , and θ stand for amplitude, period, and initial phase for a single harmonic. The quantity φ is latitude, and the shear is 5 cm s^{-1} per degree latitude in Test IV.

	Test I	Test II	Test III	Test IV
Constant zonal mean flow (cm s^{-1})	4	4	4	4
Zonal harmonic oscillations	No	$A = 4 \text{ cm s}^{-1}$	$A = 3 \text{ cm s}^{-1}$ $T = 365 \text{ days}$ $\theta = -1.64$	$A = 4 \text{ cm s}^{-1}$ $T = 45 \text{ days}$ $\theta = -1.64$
		$T = 45 \text{ days}$ $\theta = 0$	$A = 2 \text{ cm s}^{-1}$ $T = 182.5 \text{ days}$ $\theta = -0.85$	$A = 4 \text{ cm s}^{-1}$ $T = 45 \text{ days}$ $\theta = -0.85$
Mean flow shear	No	No	No	5φ

thus do not covary with each other, yielding near-zero estimated asymmetric components of diffusivity (κ_{xy} and κ_{yx}). These results confirm that our stochastic tracking model Eqs. (1) and (2) and the estimation of eddy diffusivity using Eq. (4) as well as a simple binning technique work well in a completely homogeneous and stationary flow.

In Test II, the nonstationary $U(t)$ is implemented by adding a single oscillating signal to the uniform mean flow:

$$U(t) = U_m + A \sin\left(\frac{2\pi t}{T} + \theta\right),$$

with the amplitude $A = 4 \text{ cm s}^{-1}$, period $T = 45$ days, and phase $\theta = 0$. The velocity $U_m = 4 \text{ cm s}^{-1}$ is the constant background mean as in Test I. For simplicity, only the zonal component of the flow is considered (Fig. 2a) and discussed hereafter.

Two techniques are used to estimate $U(t)$. The first method is the classical binning method, in which U is obtained by grouping drifter observations into 2° geographic bins and then averaging all observations within each bin. The second method is the seasonal binning technique, in which several seasons (temporal bins) are used, and U is estimated for each individual season. Here, two (6 months each) and four seasons (3 months each) will be considered for comparison. Finally, diffusivity is computed using u' corresponding to the different $U(t)$.

The estimated zonal velocity autocovariance from the different methods are shown in Fig. 2b. The results from the different methods are indistinguishable. The estimated autocovariance decreases within ~ 22 days and then oscillates around the analytic result. This is not surprising for the classical binning method because it completely overlooks the sinusoid signal contained in U . Thus, when doing the scale separation $u' = u - U$, this signal is not removed and resides in u' , making the velocity autocovariance oscillate around the true value

with period $T = 45$ days. For the seasonal binning method, two-season (four-season) binning is only able to resolve signals with periods longer than 1 yr (half year). Thus, for this sinusoid, results from the seasonal binning method would not be better than those from the simple binning method. Such oscillated autocovariance will of course yield an oscillated diffusivity (Fig. 2c) according to Eq. (4).

In Test III, two more realistic sinusoids are added, one with $A = 3 \text{ cm s}^{-1}$, $T = 365$ days, and $\varphi = -1.64$ to mimic the annual cycle and the other with $A = 2 \text{ cm s}^{-1}$,

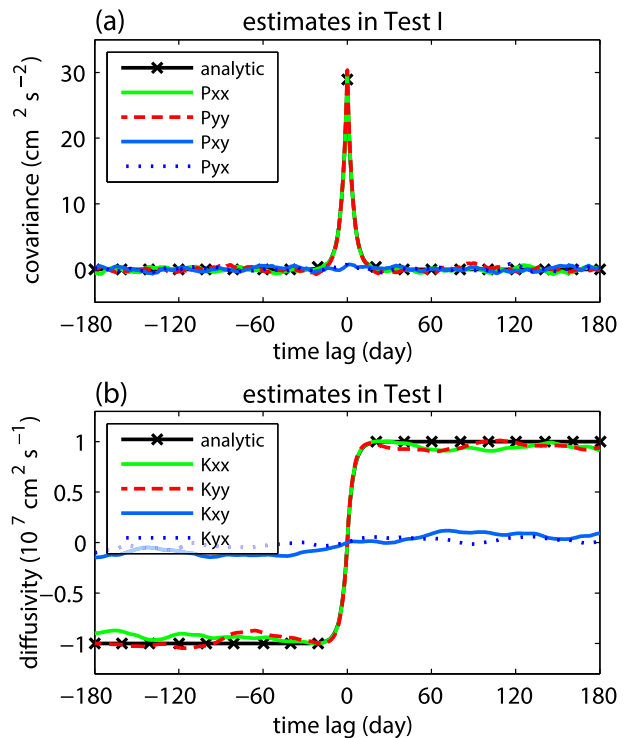


FIG. 1. Estimates of (a) velocity covariance ($\text{cm}^2 \text{s}^{-2}$) and (b) lateral eddy diffusivity ($10^7 \text{ cm}^2 \text{s}^{-1}$) as a function of time lag using the binning technique in Test I, in which a uniform zonal mean flow $U = 4 \text{ cm s}^{-1}$ is specified. Black lines show the analytic solutions for the symmetric components P_{xx} , P_{yy} , κ_{xx} , and κ_{yy} .

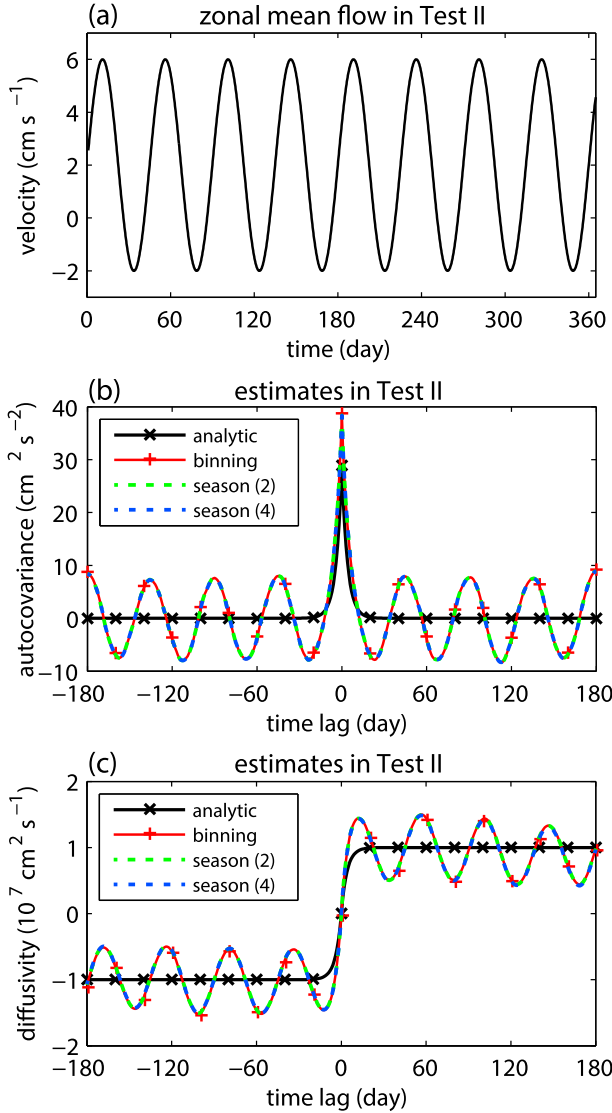


FIG. 2. (a) Evolution of background zonal mean flow U (cm s^{-1}) in Test II. (b) The estimated zonal autocovariance ($\text{cm}^2 \text{s}^{-2}$) and (c) eddy diffusivity ($10^7 \text{ cm}^2 \text{s}^{-1}$) using different methods in Test II.

$T = 182.5$ days, and $\varphi = -0.85$ to mimic the semiannual cycle (Fig. 3a). The estimated velocity covariance (Fig. 3b) using simple binning and two-season binning decreases and approaches the analytic result within several days. Then the decreasing rates of both curves slow down and make the first zero-crossing at about 65 days. Such a behavior of velocity covariance yields a dramatic increase in the corresponding diffusivities within 65 days and then a decrease similar to a sinusoid with a period of 1 yr (only a half period is shown in Fig. 3c). When the temporal bin is increased to four seasons, the effects of the annual cycle are isolated quite well but the effects of the semiannual cycle still make the estimate oscillate with a period of half a year (green line in Fig. 3c).

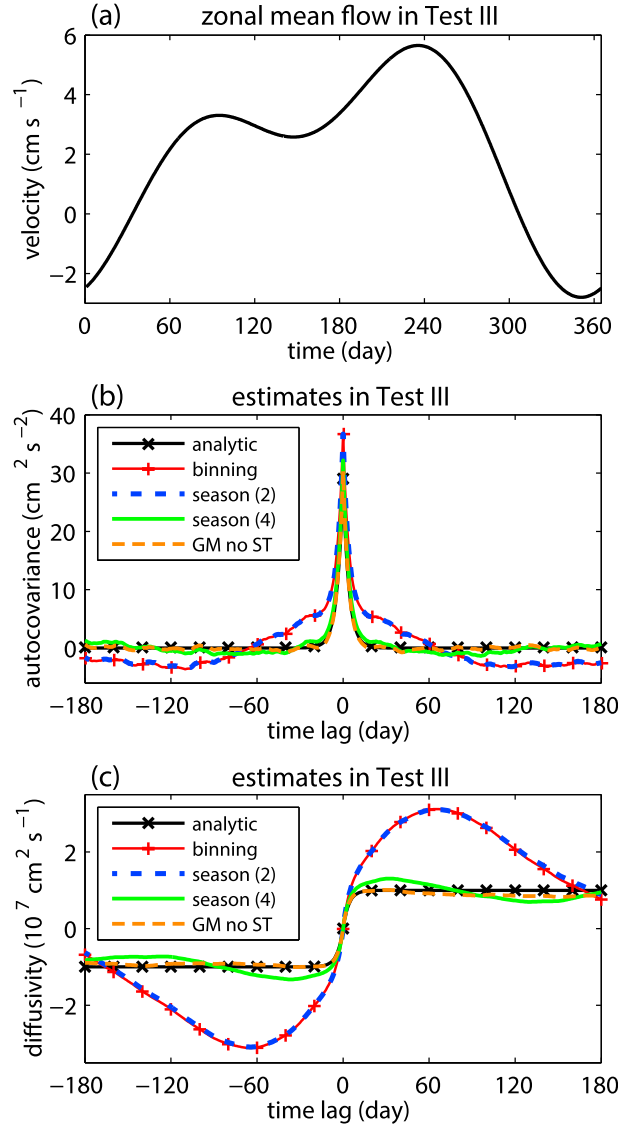


FIG. 3. As in Fig. 2, but for Test III.

Since seasonal binning only partially resolves the continuous signal $U(t)$ and increasing the number of seasons in the binning only reduces the “leakage” of the oscillating signals into u' , the corresponding diffusivities still has oscillating behavior. Thus, we use the GM estimator [Eq. (7)] to provide a continuous estimation of $U(t)$. In Eq. (7), the diagonal elements of \mathbf{R}_z are assigned to the squared half range of \mathbf{u} , while off-diagonal elements are set to zero. Elements in \mathbf{R}_n are determined by Eq. (3):

$$\mathbf{R}_n(\tau) = \sigma^2 \exp(-\tau/T_L),$$

where σ^2 is the sample variance of the velocity component within a bin. As U is homogeneous here, the spatial terms in Eq. (6) are not included [similar to Lumpkin

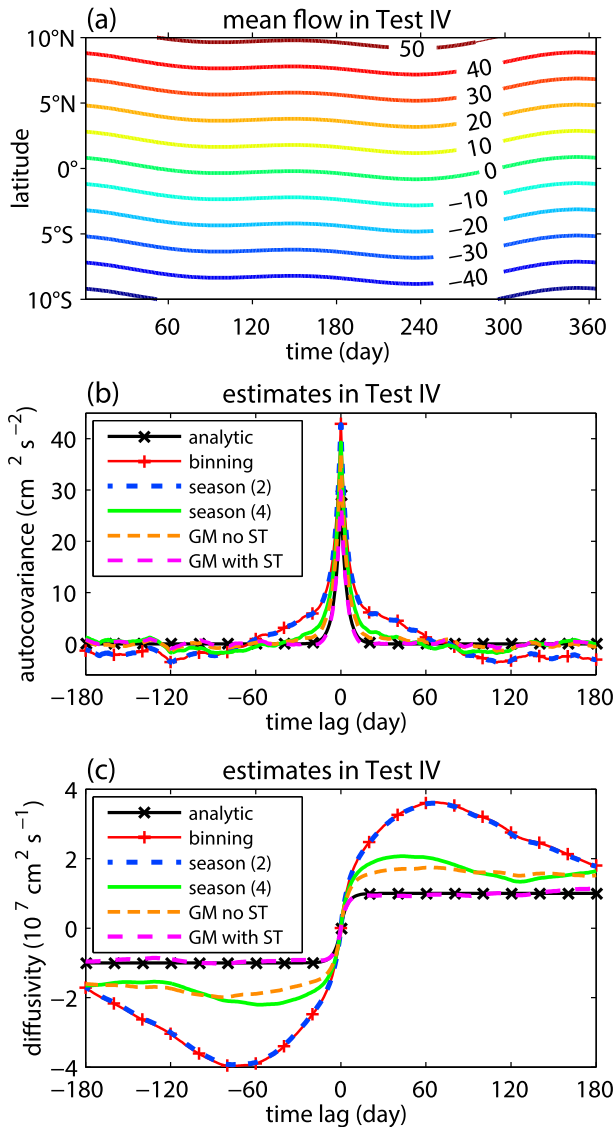


FIG. 4. (a) Latitude-time plot of background zonal mean flow U (cm s^{-1}) in Test IV. (b) The estimated zonal autocovariance ($\text{cm}^2 \text{s}^{-2}$) and (c) eddy diffusivity ($10^7 \text{cm}^2 \text{s}^{-1}$) using different methods in Test IV.

(2003)]. The GM method resolves and excludes both cycles in $U(t)$ successfully, resulting in a much more accurate u' , and hence providing the best estimates of velocity covariance and diffusivity that are almost identical to the analytic solution.

In Test IV, the situation becomes a little more complex. Spatial shear equal to 5φ (where φ is the latitude in degrees) along the meridional direction is added in addition to the constant mean and the seasonal cycle. Then $U(\mathbf{x}, t)$ is not only nonstationary but also inhomogeneous (Fig. 4a). To isolate the effect of the horizontal shear of the mean flow, spatial terms (ST) are included in the GM

method [the last five terms in Eq. (6)] to obtain the mean flow (Figs. 4b,c). Similar to those in Test III, estimates of diffusivity from the simple binning and two-season binning methods oscillate with a period of ~ 200 days (Fig. 4c), while that from the four-season binning method oscillates with a period of half a year. The GM method without ST is capable of resolving the oscillating $U(t)$, but cannot suppress the shear-induced dispersion, yielding a larger value ($\sim 1.7 \times 10^7 \text{cm}^2 \text{s}^{-1}$) after 20 days. Note that the shear dispersion is partially resolved even without ST because of the spatial binning technique and the unresolved part of shear is inside bins. If no binning is applied, the estimated diffusivity will not asymptote to a constant at all (e.g., Bauer et al. 1998) since its velocity spectrum is red (see blue solid line in Fig. 5a). With the ST included, the GM method is able to resolve both the seasonal variation and spatial shear of $U(\mathbf{x}, t)$ simultaneously, resulting in more accurate eddy velocity and the best estimate of diffusivity (Fig. 4c).

It is also interesting to see the Lagrangian velocity spectra in Test IV since the eddy-mean flow decomposition is based on the assumption of the existence of a spectra gap between large- and small-scale motions. Figure 5a shows the zonal velocity spectral density by removing U estimated by the different techniques. The analytic spectral density (thin black line in Fig. 5a) is the Fourier transform of Eq. (3):

$$S(f) = \int_{-\infty}^{\infty} P(\tau) e^{-i2\pi f\tau} d\tau = \frac{2\kappa^\infty}{1 + (2\pi f T_L)^2},$$

where f is the frequency in units of cycles per day (cpd). Its slope on the log-log plot is

$$Y(f) = \frac{d \ln S(f)}{d \ln f} = -\frac{2}{1/(4\pi^2 T_L^2 f^2) + 1}.$$

Therefore, the slope approaches -2 as the frequency goes to infinity. On the other hand, the spectra become white ($Y \rightarrow 0$) when $f \rightarrow 0$, forming a spectrum plateau. Spectra from all methods agree well with the analytic one except at very low and high frequencies. The deviation at the high-frequency end is due to the discretization of Eqs. (1)–(2) with a finite sampling rate $\Delta t = 1/4$ day. The deviation at the low-frequency end is more important and would affect the estimation of diffusivity because

$$\kappa^\infty = - \int_0^{\infty} P(t) dt = \frac{1}{2} S(0).$$

This is why a time-invariant mean flow ($f = 0$) should be removed as the diffusivity is determined by the lowest frequency of motion. The spectrum of original velocity

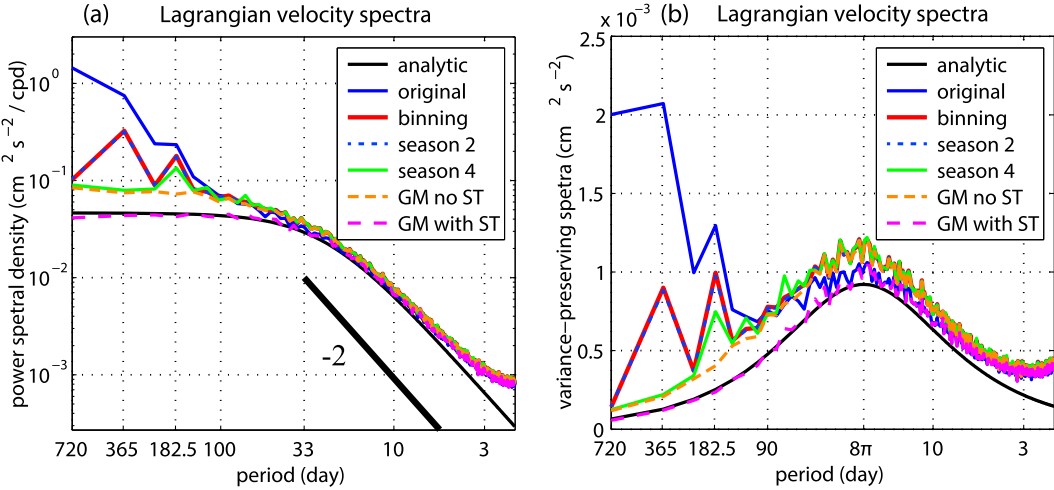


FIG. 5. Lagrangian zonal velocity (a) power spectral density ($\text{cm}^2 \text{s}^{-2} \text{ cpd}^{-1}$) on a log–log plot and (b) variance-preserving spectra ($\text{cm}^2 \text{s}^{-2}$) on a semilog plot in Test IV. The thick black line in (a) indicates a slope of -2 .

(blue solid line in Fig. 5), containing spatial shear (inhomogeneity) and low-frequency variabilities (nonstationarity), is obviously red even at periods longer than 100 days. The simple binning and the two-season binning methods are capable of partially reducing the shear effect, but incapable of reducing the two spectral peaks associated with the annual (365 days) and semiannual (182.5 days) cycles. The four-season binning method removes the annual peak but only slightly reduces the semiannual peak. The GM method without ST has successfully removed the two peaks but fails to reduce the shear inside bins, leaving the spectra at low frequencies slightly red. When ST is added, the GM method produces a nearly perfect spectrum that coincides with the analytic one.

Figure 5b shows the variance-preserving spectra (spectral density multiplied by f), in which the area under the curve represents the variance (or, equivalently, energy) contribution of each frequency band to the total variance of the series (Emery and Thomson 2001). The energy-containing band peaks at $2\pi T_L$ and decays toward the two ends of the spectrum. It is found that the variance contributions of both the seasonal cycle and the mean flow shear in the low-frequency band (> 90 days) are comparable to (or even larger than) the energy-containing eddies (pink line in Fig. 5b), which depend on the prescribed parameters of seasonal cycle amplitude and diffusivity. The GM method with ST included has isolated their contributions successfully.

Note that the GM method performs near perfectly in these cases. This is because the mean flow is designed consistently with Eq. (6), that is, a linear combination of temporal and spatial variations by assuming stationary spatial variation and homogeneous temporal variation.

These mean flows are intentionally designed so that we can clearly see different performances of methods caused only by the nonstationarity of the mean flow rather than other factors. Actually, there are also many cases in which the GM method performs not so well or even fails. For example, the spatial variation of the mean flow follows higher-order (third order) polynomial variation rather than the second-order form used in Eq. (6) or even nonpolynomial variations (e.g., exponential variation). Besides, if the shear strength changes with time (nonstationary spatial variation) or amplitude of temporal variation changes with space (inhomogeneous temporal variation), that is, the prescribed form in Eq. (6) does not exactly apply, the GM method is likely to fail in fitting such mean flows. Fortunately, if the GM method is used in conjugation with the spatial binning technique (domain is divided into smaller bins), the performance of the GM would improve because homogeneity is approximately valid inside a smaller bin. Thus, the second-order polynomial fit in Eq. (6) is good enough to resolve any kind of nonsharp spatial variation inside a smaller bin, and the amplitude of temporal variation will also remain roughly a constant. The GM performance in these cases will be shown in the next section through more realistic tests in which the mean flows are derived from satellite-based observations without prescribed forms.

Conclusions can now be drawn from the above idealized tests. If U is nonstationary (even if it is homogeneous), containing low-frequency variabilities such as a seasonal cycle, the classical binning method cannot provide an accurate estimation of diffusivity but will instead produce an oscillating estimate. The oscillating behavior depends on the amplitudes, periods, and phases of the signals.

Although the positive and negative lobes around the analytic velocity autocovariance (e.g., Fig. 2b) seem to cancel each other as time approaches infinity, making no net contribution to the asymptotic diffusivity, they would bias the diffusivity and make the estimation increase at relatively short time lags. In practice, estimates are usually done within several tens of days, for example, below a month for energetic or small-scale basins (e.g., Andersson et al. 2011; Bauer et al. 2002; Maurizi et al. 2004; Poulain 2001; Qian et al. 2013; Ursella et al. 2006) and 1 to 2 months for quiescent basins (e.g., Bograd et al. 1999; Falco et al. 2000; Swenson and Niiler 1996; Zhang et al. 2001). Only those studies based on synthetic drifters can assess much longer time lags to several years (e.g., Banyte et al. 2013; Griesel et al. 2010). However, longer time lags may also induce the nonlocal mixing problem since drifters will sample a range of mixing behavior over several years. The seasonal binning method, viewed in a piecewise way, is capable of partially reducing the impact caused by seasonal variations but incapable of completely eliminating it (Fig. 3). Increasing the temporal resolution (more seasons are used) could approach the true solution but remain impractical because this also significantly reduces the number of samples within each season. Continuous estimation of $U(t)$ such as via the GM method provides a good remedy for the estimation of diffusivity in a nonstationary background mean flow. As for the new GM method with ST, it can isolate the effects of both nonstationarity and inhomogeneity of $U(\mathbf{x}, t)$ on estimating diffusivity.

4. Results from the OSCAR scenario

The above tests may be too idealized because the velocity spectra in real oceans may be quite different. Therefore, in this section, a more realistic scenario regarding the background flows in the Indian Ocean (IO) is considered. Synthetic drifters are deployed in currents depicted by the global Ocean Surface Currents Analyses-Real time (OSCAR) data obtained online (from www.oscar.noaa.gov). The velocity of OSCAR is directly derived from sea surface height, surface wind, and sea surface temperature collected from both satellites and in situ instruments, including geostrophic, Ekman, and Stommel shear dynamics and a term from the surface buoyancy gradient (Bonjean and Lagerloef 2002). The 5 yr of data from 2006 to 2010 are used, with 1/72-yr (5 days) temporal and $1/3^\circ$ spatial resolutions. Only the Indian Ocean is examined here (50°S – 30°N , 20° – 120°E ; Fig. 5) because of strong seasonal cycle within this region. Notice that the Rossby radius and thus the scale of eddies gets small at 50°S , and so the satellite altimetry (and the OSCAR data) would tend to underestimate the

in situ eddy kinetic energy at the southern edge of our domain. However, as this only affects the southernmost part of the domain, results shown here are not sensitive to this.

This OSCAR scenario is different from the previous idealized scenario in several aspects. First of all, the velocity spectra of the OSCAR data range from meso-scale to interannual variabilities that are expected to be closer to reality than in the previous scenario. The second aspect is that not only the amplitude and phase of the seasonal cycle vary with space (inhomogeneous temporal variation), but also the shear strength would change with time (nonstationary spatial variation). Therefore, no prescribed mathematical form of the mean flow is assumed. Third, only segments of Lagrangian observations contain the seasonal signal when drifters traveled over the region of strong seasonal cycle, which is different from the earlier scenario.

The deployment strategy is as follows. Synthetic drifters are released in four patches each year (one patch every 3 months). Drifters in each patch are deployed simultaneously at a uniform 1.5° latitude/longitude interval over the whole basin and then tracked for half a year using Eq. (1) with $\kappa^\infty = 1 \times 10^3 \text{ cm}^2 \text{ s}^{-1}$ and $T_L = 4$ days. Such a tiny diffusivity value (as compared to $\kappa^\infty = 1 \times 10^7 \text{ cm}^2 \text{ s}^{-1}$ in idealized tests) is only used to introduce a random movement of drifters without affecting the velocity spectra of the OSCAR data, so that drifters follow different pathways even if they are deployed at exactly the same initial location. OSCAR data are first linearly interpolated into daily data and drifter velocities are recorded every day. Tracking is stopped if a drifter moves onto land.

Figure 6 shows the number of daily observations in 2° bins after 6-yr simulations. The southern IO and the eastern equatorial IO are heavily sampled, whereas the western equatorial IO and the coastal regions are sampled less. For most parts of the IO, the number of daily observations is above 2000. As the drifters are deployed regularly (one patch every 3 months), drifter observations in each season would be roughly equal, and no significant seasonal sampling bias exists. On the other hand, drifters are deployed uniformly in space, and the array bias caused by nonuniform drifter observations should be partially reduced. However, Fig. 6 shows that drifter numbers also vary from bin to bin and such distribution is probably attributed to the divergence/convergence of OSCAR currents. Therefore, following Poulain (2001), the array bias is computed by assuming constant zonal ($20 \times 10^7 \text{ cm}^2 \text{ s}^{-1}$) and meridional ($10 \times 10^7 \text{ cm}^2 \text{ s}^{-1}$) diffusivities. Results (figure not shown) show that in the ocean interior, array biases are below 1 cm s^{-1} , except for the western equatorial regions where bias remains below

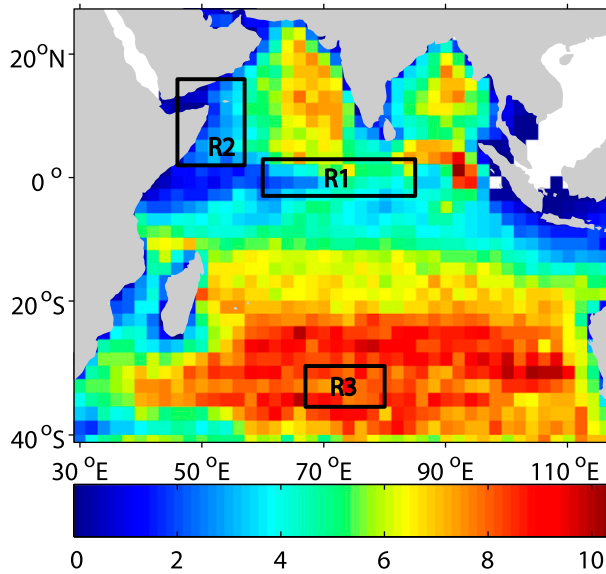


FIG. 6. Number of daily synthetic drifter observations (10^3) in 2° bins after 5-yr simulation using OSCAR data. Black boxes define three regions for the estimates of diffusivity.

4 cm s^{-1} . This is relatively small as compared to the mean flow shown in Fig. 7 and would not much affect the results.

First, we will validate the estimate of the mean flow $U(\mathbf{x}, t)$ using the new GM method with ST included against the “true” mean derived from OSCAR data. The true mean defined here consists of a time-invariant Eulerian mean and a seasonal cycle (including annual cycle and semiannual cycle). The time-invariant Eulerian mean is a simple temporal average from 2006 to 2010, and the seasonal cycle is computed using a least squares fit of annual and semiannual sinusoids at each grid. For the GM estimates, the time-invariant mean, seasonal cycle, as well as ST are all included in Eq. (6) using 2° bins, and elements of \mathbf{R}_n in Eq. (7) are computed following Lumpkin (2003):

$$\mathbf{R}_n(\tau) = \sigma^2 \cos\left(\frac{\pi\tau}{T_d}\right) \exp\left[-\left(\frac{\pi\tau}{2\sqrt{2}T_d}\right)^2\right],$$

where σ^2 is the sample variance of the velocity component within a bin and $T_d \approx 8.27$ days, consistent with an integral eddy time scale of 4 days. The matrix \mathbf{R}_z is identical to that in idealized Tests III and IV.

Figure 7 shows the spatial mean $U(\mathbf{x})$ obtained from the above two approaches. Although the resolutions are different, both means agree quite well with each other. Figure 8 shows the amplitude of the annual cycle from the two methods. Ignoring those unreliable results within the South China Sea region due to sparse samples, the

estimates also agree well with each other. The Somali Current, driven by the annually reversing Indian monsoon, exhibits significant annual variation where both zonal and meridional amplitude maxima are located. Large zonal amplitudes also occur in the equatorial region, extending from the African coast to $\sim 75^\circ\text{E}$ and then shifting north to south of India as well as south-southeast of Sri Lanka, where the currents are influenced by monsoon winds switching annually between summer (southwest) and winter (northeast). South of 10°S , the amplitude of the annual cycle is quite weak. For the semiannual cycle (Fig. 9), the zonal amplitude maxima are located almost along the equator, extending from coast of Africa to $\sim 90^\circ\text{E}$, while the meridional ones are trivial, indicating the semiannual variation mainly exists in the equatorial jet occurring twice a year during the intermonsoon periods.

The above comparison proves that the GM method with ST is capable of reproducing the true $U(\mathbf{x}, t)$. Based on the above analysis, three subregions are defined (see Fig. 6) within which drifter observations are used as the origins of pseudotracks for diffusivity estimation. Region 1 [equatorial (EQ)] is centered in the equatorial region where both annual and semiannual cycles are strong (Figs. 8, 9). Region 2 [western boundary (WB)] covers the western boundary current (i.e., the Somali jet) where the annual cycle is strong. Region 3 [southern Indian Ocean (SIO)] is located in the relatively quiescent region in the southern Indian Ocean where the seasonal cycle is quite weak.

For the OSCAR scenario, there is no analytic solution for comparison as in the idealized scenarios. We could nevertheless define a true diffusivity by taking the advantage of the exactly known Eulerian field. The inhomogeneous and nonstationary mean flow $U(\mathbf{x}, t)$ is defined as the sum of the time-invariant Eulerian mean from 2006 to 2010 and a seasonal cycle reconstructed by least squares fit at each grid. The residual velocity of synthetic drifters for computing true diffusivity is relative to this $U(\mathbf{x}, t)$.

The true and estimated diffusivities from the different methods are shown in Fig. 10. In view of the asymptotic nature, the true diffusivities of both zonal and meridional components over the three regions all approach some steady values at larger lags and thus could be used as references for the estimates from different techniques. At first glance, the classical binning method gives the largest estimates (in magnitude), followed by the two-season binning method. The four-season binning and GM with ST methods provide estimates quite close to the true diffusivity, especially in the EQ and WB regions where the seasonal signal is significant (Figs. 10a–d). In the SIO region where the seasonal cycle is negligible, the four

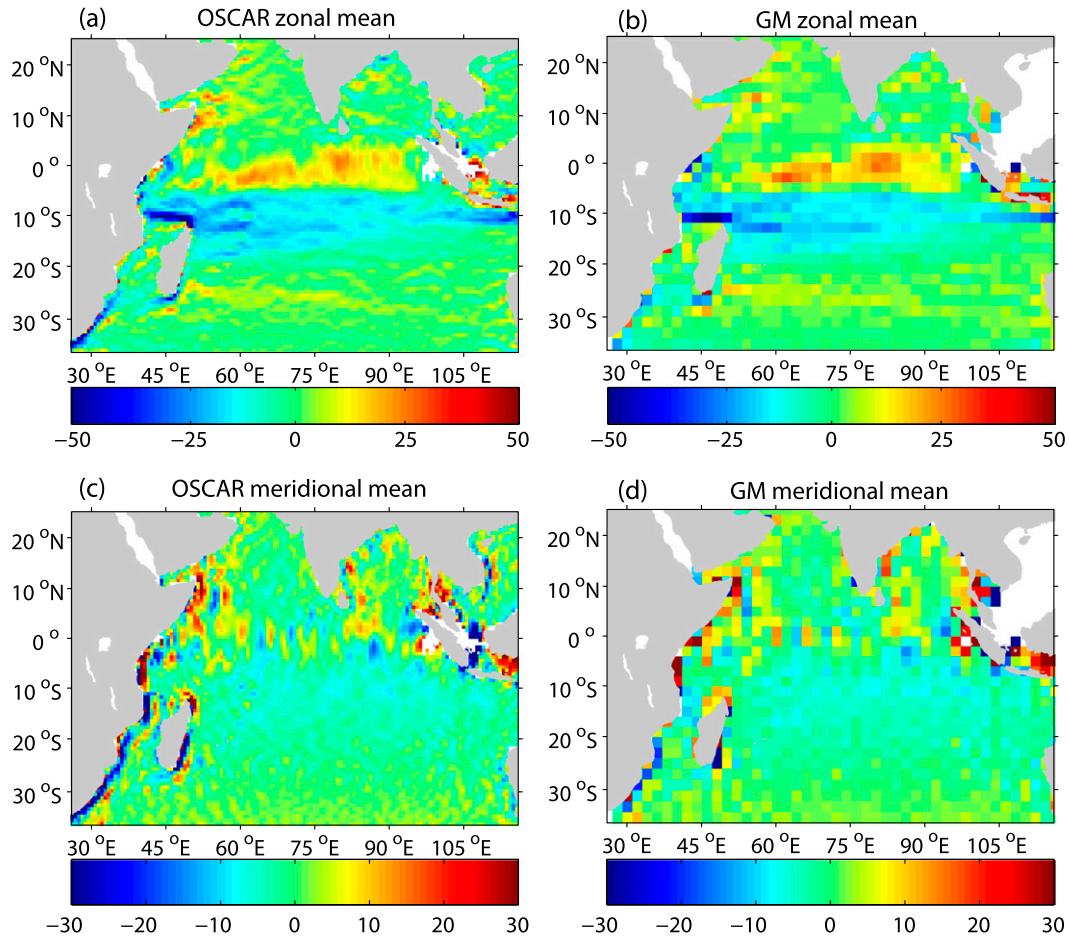


FIG. 7. (a) Zonal and (c) meridional components of surface mean flows (cm s^{-1}) derived from the OSCAR 2006–10 mean. (b),(d) As in (a),(c) but derived from synthetic drifters grouped into 2° bins using the GM method with ST.

methods produce similar estimates to the true diffusivity. Conclusions from previous idealized tests can also be validated here. In the EQ region, for example, where the seasonal cycle is strong, the estimate from the classical binning method seems to have a complete wave trough/ridge within half a year, indicating an oscillation with a period of 1 yr (see negative time lags in Fig. 10a and positive time lags in Fig. 10c). The two-season binning method also provides a similar estimate but the amplitude is reduced. The meridional estimates in the EQ and WB regions (Figs. 10b,d) show less oscillating characteristics, but the asymptotic values from the classical binning method (or two-season binning method) are also much larger than those from the GM method with ST (or true). Increasing the temporal bins to four seasons further reduces the oscillating features and makes the corresponding estimate much closer to the true diffusivity. However, apparent differences between the estimate by the four-season binning method and the true diffusivity can also be found in both the EQ and WB regions, especially in

the meridional component (Figs. 10b, 10d). The GM method with ST included performs best and provides an estimate that never deviates far from the true diffusivity.

This conclusion also applies to the SIO region, but the differences are much smaller since the seasonal signal in this region is quite weak (Figs. 8, 9). Thus, the simple binning method would yield a reasonable result. To our surprise, for the zonal component (Fig. 10e), all methods (even the true diffusivity) provide results that only marginally asymptote to constant values after 90 days. In addition, the meridional estimates overshoot at 15 days and then level off to a constant after 50 days (Fig. 10f), indicating a significant negative lobe in the autocovariance function that is usually observed in cross-stream estimates (e.g., Bauer et al. 2002; Griesel et al. 2010; Klocker et al. 2012). These features are likely attributed to the low-frequency (Rossby) waves resolved by OSCAR data, which is in line with the description by Klocker et al. (2012).

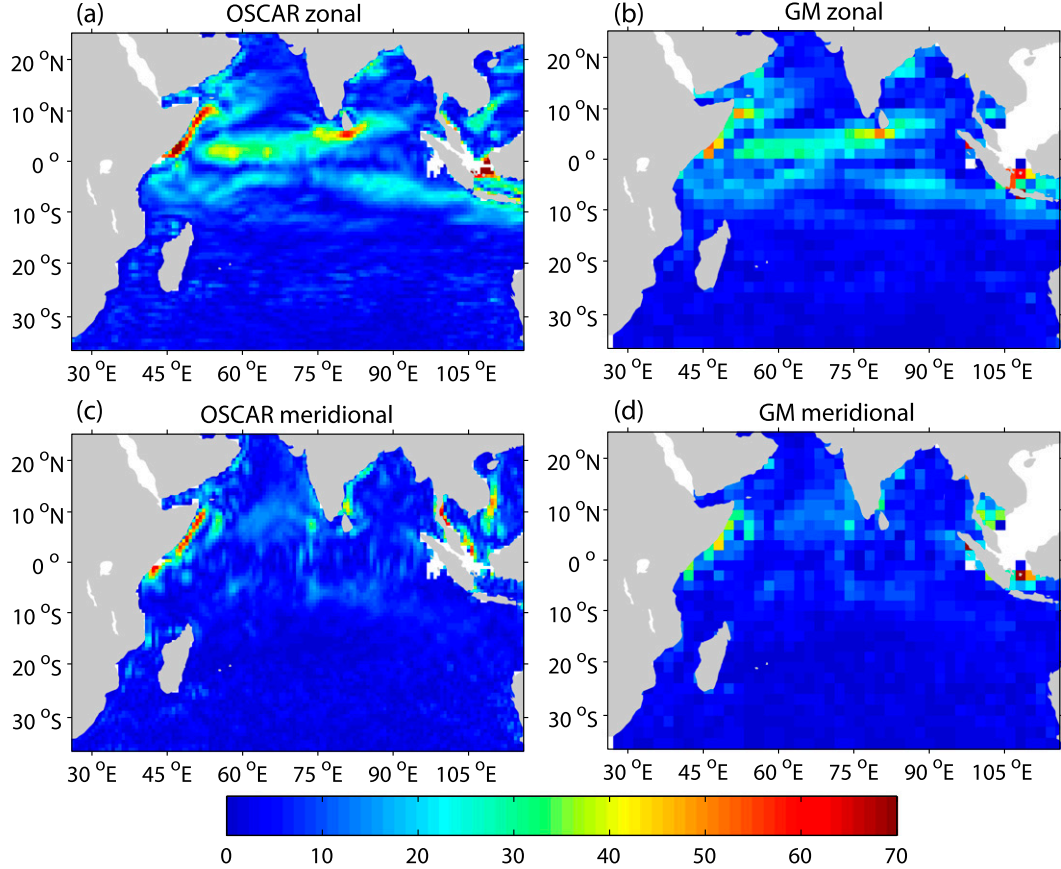


FIG. 8. (a) Zonal and (c) meridional amplitudes (cm s^{-1}) of the annual cycle of surface flows derived from the 2006–10 OSCAR data using a least squares fit. (b),(d) As in (a),(c) but derived from synthetic drifters grouped into 2° bins using the GM method with ST.

5. Conclusions and discussion

To demonstrate the effects of a nonstationary mean flow on the estimation of Lagrangian diffusivity, two scenarios are designed in the present study. In the first scenario, synthetic drifters are deployed in a completely idealized mean flow that consists of a time-invariant part and a sinusoidal oscillated part. When decomposing the velocities sampled by drifters into eddy and mean components using the classical binning method, the oscillating part of the mean flow leaks into the eddy component, resulting in an oscillating estimate of diffusivity. Using a temporal binning method such as the seasonal binning method can partially resolve the nonstationary part of the mean flow and thus reduce the amplitude of oscillation in the estimated diffusivity. The new GM method (with spatial terms included) proposed by Lumpkin and Johnson (2013), fitting the mean flow in a continuous sense, gives the best estimate of diffusivity even when the mean flow is both nonstationary and inhomogeneous. Although the seasonal variability does

not have a net contribution to the dispersion, it may cause large bias in the estimate of diffusivity within a time lag of ~ 2 months, especially when the classical binning method is used.

In the second scenario, a large number of synthetic drifters are released in the ocean currents in the IO basin prescribed by the 2006–10 OSCAR product. This scenario is more complex than the idealized one, and the velocity spectra from the former are expected to be closer to real oceanic conditions. In this case, the inhomogeneous and nonstationary Eulerian mean flow is exactly defined by OSCAR regular-gridded data. Hence, a true diffusivity could be computed using residual velocities with respect to the true Eulerian mean. When estimating diffusivities over regions where the seasonal cycle is strong (e.g., equatorial and western boundary regions), the classical binning method gives the largest estimates that increase within 2 months, showing an oscillating behavior similar to that in the idealized scenario. The two-season binning method reduces the magnitude of oscillation, while the four-season binning method

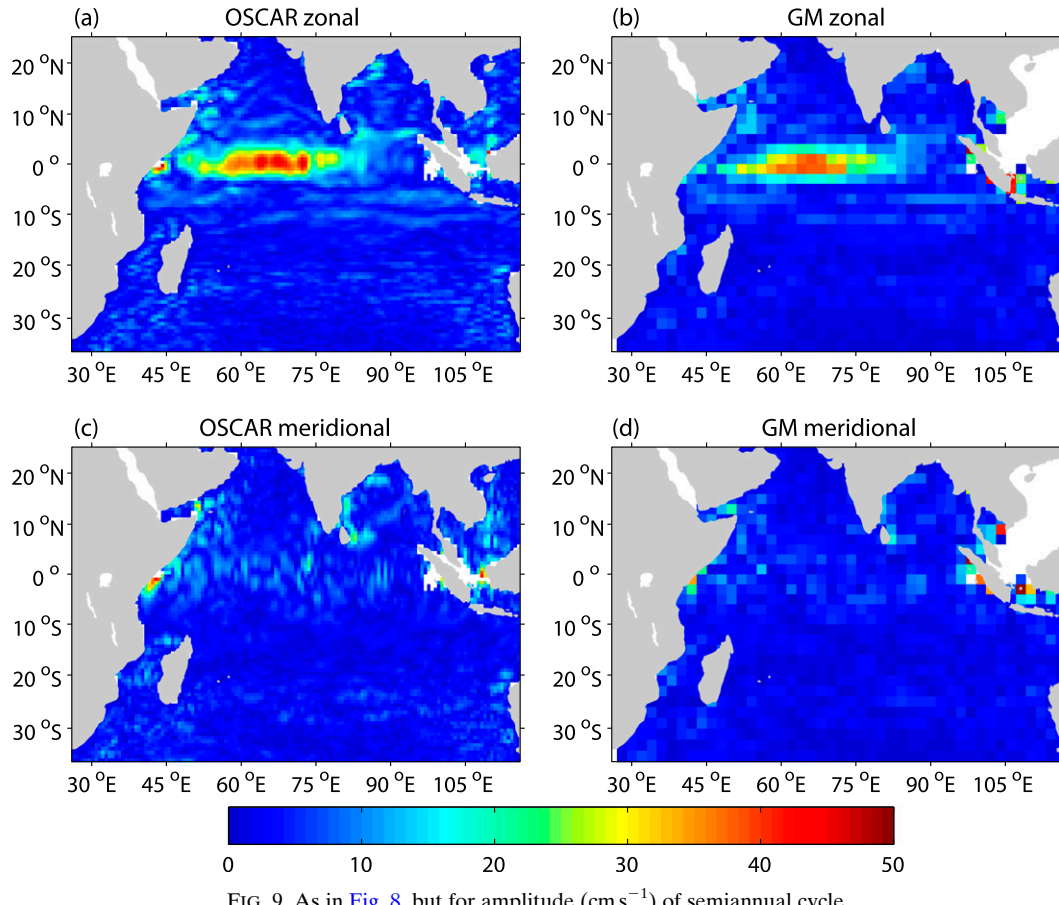


FIG. 9. As in Fig. 8, but for amplitude (cm s^{-1}) of semiannual cycle.

provides acceptable results. The new GM method with ST included successfully captures the temporal variation as well as spatial variation of the mean flow, resulting in a quick convergence of estimates to the true diffusivity, especially in the eastern coast of Somalia and the equatorial IO where a strong signal of seasonal cycle exists in the surface currents influenced by the monsoon winds. For the region over the southern IO where seasonal variation is weak, the simple binning method is sufficient to give a result close to the true diffusivity.

The seasonal cycle focused on here is not the only signal that contributes to the nonstationary mean flow. At a shorter time scale, as shown in Fig. 11, there are also triannual (~120 days) peaks in the zonal velocity over the EQ and WB regions besides the annual and semiannual spikes. Actually, if trapped by a strong rotational eddy field, the autocovariance of a drifter would also show the oscillation feature (e.g., Veneziani et al. 2005). Therefore, at a longer time scale (cannot be shown in Fig. 11), interannual variability might also exert some influence on diffusivity estimation.

On the other hand, the present study only discusses the nonstationarity of $U(t)$. It should be noted that the

statistical properties of u' are also nonstationary (e.g., diffusivity varies with time). In this situation, the seasonal binning technique is quite suitable for temporal analysis. For example, Andersson et al. (2011) provided diffusivities in summer and winter over the Nordic Seas using the two-season (6 month each) binning technique. Nevertheless, removing a nonstationary $U(t)$ (as emphasized in this study) may provide more accurate u' statistics.

It is worth mentioning the strategy used by several studies (e.g., Krauss and Böning 1987; Lumpkin et al. 2002; Rupolo 2007) in which drifters are divided into equal length segments and then the Lagrangian mean and linear trend of segments are removed to obtain the residual velocity for diffusivity estimation. This approach cuts off the velocity spectrum at a specific period, and variabilities longer than that period are excluded naturally. Rupolo (2007) used 64-day segments that filter out the impact of seasonal and interannual variabilities much longer than 64 days. If the spectral plateau can be reached at 64 days (become a white spectrum), the true diffusivity could converge. If the spectrum was still red, no diffusivity would exist (LaCasce 2008). Velocities over some regions (e.g., the equatorial region) might be red at the cutoff period

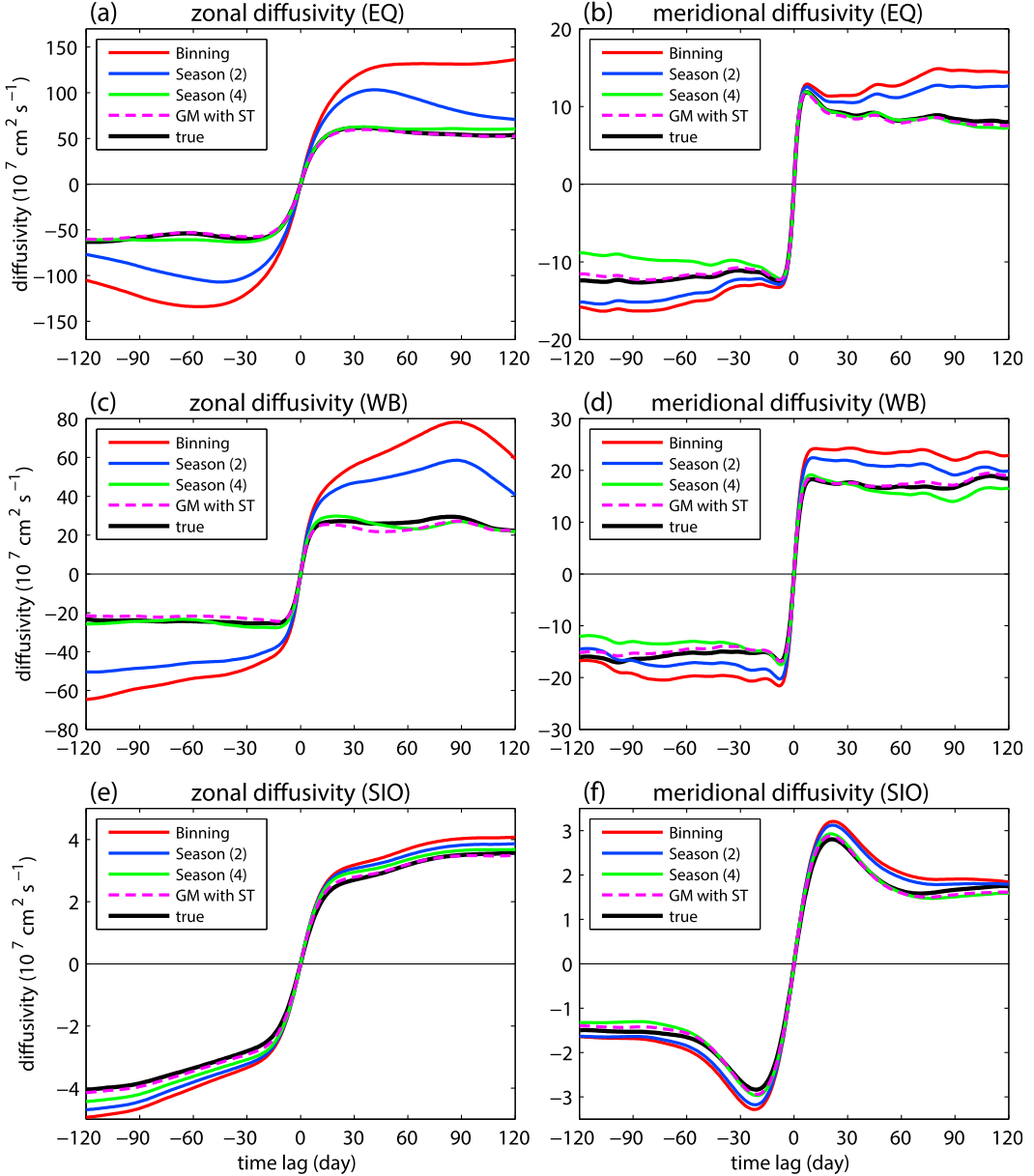


FIG. 10. Estimated (left) zonal and (right) meridional diffusivity ($10^7 \text{ cm}^2 \text{ s}^{-1}$) using different methods for (a),(b) region 1 (EQ), (c),(d) region 2 (WB), and (e),(f) region 3 (SIO) defined in Fig. 6.

(Fig. 11). Increasing the cutoff period, such as in Lumpkin et al. (2002), who used 120-day segments, however, would face the potential problems of fewer segments.

Recently, discrepancies between diffusivity estimates from different methods are reported, especially those from drifter-based and tracer-based methods. While many studies have obtained larger values from drifter-based methods than those from tracer-based methods (e.g., Chiswell 2013; Lumpkin and Pazos 2007; Sallée et al. 2008; Sundermeyer and Price 1998), Klocker et al. (2012) has shown that the overestimated diffusivities

from drifter-based methods would be reduced to agree with those from tracer-based methods when using sufficiently long times. The present study demonstrated that if the seasonal variability is removed from residual velocity, the magnitude of estimated diffusivity would also be reduced significantly for monsoon-dominated regions (also see Zhurbas et al. 2014). Another benefit of isolating the seasonal variability is that the estimates quickly converge to the true diffusivity. This may help to obtain the asymptotic value of diffusivity estimate in a relatively short time using real drifter data, since long

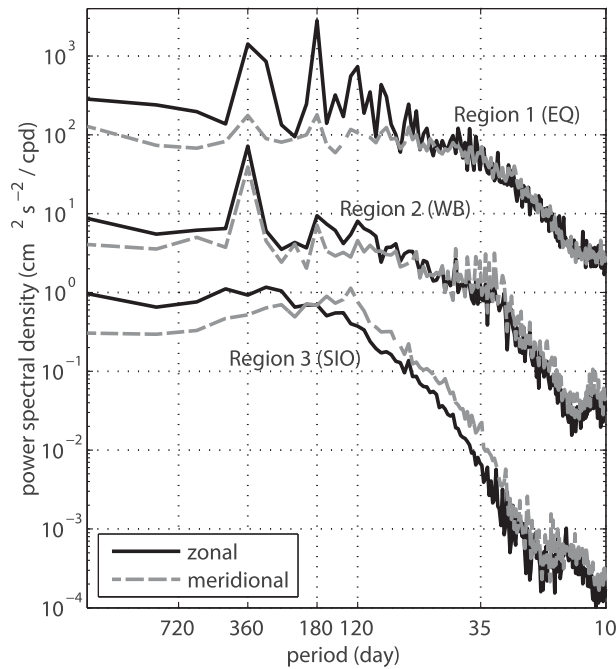


FIG. 11. Eulerian spectra ($\text{cm}^2 \text{s}^{-2} \text{cpd}^{-1}$) averaged over all grids within the three regions defined in Fig. 6. The spectra of region 1 (EQ) is shifted up by multiplying by 50 for a clear view.

time assessment (e.g., several months) is usually unpractical for the real drifter due to error increments (Davis 1991) and nonlocality (drifters would move outside the domain of interest). But one should be aware of other factors affecting the short time estimates of diffusivity such as the presence of Rossby waves. These waves tend to inhibit dispersion across the meridional mean vorticity gradient and are not resolved in the mean flow we remove, potentially complicating the diffusivity for small lags.

As already shown in the present study, nonstationary, as well as inhomogeneous, mean flows exert some influence on diffusivity estimates. Scale-separation methods should take them into account if they cannot be ignored. The new GM method with ST, as one of the choices but not the only, is very efficient in simultaneously removing both the seasonal variability and spatial shear of mean currents. Therefore, it is particularly appropriate for diffusivity estimation using real drifter data in those regions where significant nonstationarity and inhomogeneity exist, such as the Indian Ocean. This will be presented in our next publication.

Acknowledgments. This work is jointly supported by the Strategic Priority Research Program of the Chinese Academy of Sciences (XDA11010304), the MOST of China (2011CB403505, 2010CB950302), the Knowledge Innovation Program of the Chinese Academy of Sciences

(SQ201305), and National Natural Science Foundation of China (41376021, 41306013), the Hundred Talent Program of the Chinese Academy of Sciences. The authors gratefully acknowledge the use of the HPCC at the South China Sea Institute of Oceanology, Chinese Academy of Sciences. R. Lumpkin was supported by NOAA's Climate Program Office and the Atlantic Oceanographic and Meteorological Laboratory.

REFERENCES

- Andersson, M., K. A. Orvik, J. H. LaCasce, I. Koszalka, and C. Mauritzen, 2011: Variability of the Norwegian Atlantic Current and associated eddy field from surface drifters. *J. Geophys. Res.*, **116**, C08032, doi:[10.1029/2011JC007078](https://doi.org/10.1029/2011JC007078).
- Banyte, D., M. Visbeck, T. Tanhua, T. Fischer, G. Krahmann, and J. Karstensen, 2013: Lateral diffusivity from tracer release experiments in the tropical North Atlantic thermocline. *J. Geophys. Res. Oceans*, **118**, 2719–2733, doi:[10.1002/jgrc.20211](https://doi.org/10.1002/jgrc.20211).
- Bauer, S., M. S. Swenson, A. Griffa, A. J. Mariano, and K. Owens, 1998: Eddy-mean flow decomposition and eddy-diffusivity estimates in the tropical Pacific Ocean: 1. Methodology. *J. Geophys. Res.*, **103**, 30 855–30 871, doi:[10.1029/1998JC900009](https://doi.org/10.1029/1998JC900009).
- , —, —, 2002: Eddy-mean flow decomposition and eddy-diffusivity estimates in the tropical Pacific Ocean: 2. Results. *J. Geophys. Res.*, **107**, 3154, doi:[10.1029/2000JC000613](https://doi.org/10.1029/2000JC000613).
- Bograd, S. J., R. E. Thomson, A. B. Rabinovich, and P. H. LeBlond, 1999: Near-surface circulation of the northeast Pacific Ocean derived from WOCE-SVP satellite-tracked drifters. *Deep-Sea Res. II*, **46**, 2371–2403, doi:[10.1016/S0967-0645\(99\)00068-5](https://doi.org/10.1016/S0967-0645(99)00068-5).
- Bonjean, F., and G. S. E. Lagerloef, 2002: Diagnostic model and analysis of the surface currents in the tropical Pacific Ocean. *J. Phys. Oceanogr.*, **32**, 2938–2954, doi:[10.1175/1520-0485\(2002\)032<2938:DMAAOT>2.0.CO;2](https://doi.org/10.1175/1520-0485(2002)032<2938:DMAAOT>2.0.CO;2).
- Chaigneau, A., and O. Pizarro, 2005: Mean surface circulation and mesoscale turbulent flow characteristics in the eastern South Pacific from satellite tracked drifters. *J. Geophys. Res.*, **110**, C05014, doi:[10.1029/2004JC002628](https://doi.org/10.1029/2004JC002628).
- Chiswell, S. M., 2013: Lagrangian timescales and eddy diffusivity at 1000 m compared to the surface in the south Pacific and Indian Oceans. *J. Phys. Oceanogr.*, **43**, 2718–2732, doi:[10.1175/JPO-D-13-044.1](https://doi.org/10.1175/JPO-D-13-044.1).
- Davis, R. E., 1987: Modeling eddy transport of passive tracers. *J. Mar. Res.*, **45**, 635–666, doi:[10.1357/00222408778326803](https://doi.org/10.1357/00222408778326803).
- , 1991: Observing the general circulation with floats. *Deep-Sea Res. I*, **38**, S531–S571, doi:[10.1016/S0198-0149\(12\)80023-9](https://doi.org/10.1016/S0198-0149(12)80023-9).
- De Dominicis, M. D., G. Leuzzi, P. Monti, N. Pinardi, and P.-M. Poulain, 2012: Eddy diffusivity derived from drifter data for dispersion model applications. *Ocean Dyn.*, **62**, 1381–1398, doi:[10.1007/s10236-012-0564-2](https://doi.org/10.1007/s10236-012-0564-2).
- Emery, W. J., and R. E. Thomson, 2001: *Data Analysis Methods in Physical Oceanography*. 2nd ed. Elsevier, 638 pp.
- Falco, P., and E. Zambianchi, 2011: Near-surface structure of the Antarctic Circumpolar Current derived from World Ocean circulation experiment drifter data. *J. Geophys. Res.*, **116**, C05003, doi:[10.1029/2010JC006349](https://doi.org/10.1029/2010JC006349).
- , A. Griffa, P.-M. Poulain, and E. Zambianchi, 2000: Transport properties in the Adriatic Sea as deduced from drifter data. *J. Phys. Oceanogr.*, **30**, 2055–2071, doi:[10.1175/1520-0485\(2000\)030<2055:TPITAS>2.0.CO;2](https://doi.org/10.1175/1520-0485(2000)030<2055:TPITAS>2.0.CO;2).
- Griesel, A., S. T. Gille, J. Sprintall, J. L. McClean, J. H. LaCasce, and M. E. Maltrud, 2010: Isopycnal diffusivities in the Antarctic

- Circumpolar Current inferred from Lagrangian floats in an eddy model. *J. Geophys. Res.*, **115**, C06006, doi:[10.1029/2009JC005821](https://doi.org/10.1029/2009JC005821).
- Griffa, A., 1996: Applications of stochastic particle models to oceanographic problems. *Stochastic Modelling in Physical Oceanography*, R. J. Adler et al., Eds., Birkhäuser, 113–140.
- Grodsky, S. A., R. Lumpkin, and J. A. Carton, 2011: Spurious trends in global surface drifter currents. *Geophys. Res. Lett.*, **38**, L10606, doi:[10.1029/2011GL047393](https://doi.org/10.1029/2011GL047393).
- Johnson, G. C., 2001: The Pacific Ocean subtropical cell surface limb. *Geophys. Res. Lett.*, **28**, 1771–1774, doi:[10.1029/2000GL012723](https://doi.org/10.1029/2000GL012723).
- Klocker, A., R. Ferrari, and J. H. LaCasce, 2012: Estimating suppression of eddy mixing by mean flows. *J. Phys. Oceanogr.*, **42**, 1566–1576, doi:[10.1175/JPO-D-11-0205.1](https://doi.org/10.1175/JPO-D-11-0205.1).
- Koszalka, I. M., and J. H. LaCasce, 2010: Lagrangian analysis by clustering. *Ocean Dyn.*, **60**, 957–972, doi:[10.1007/s10236-010-0306-2](https://doi.org/10.1007/s10236-010-0306-2).
- Krauss, W., and C. W. Böning, 1987: Lagrangian properties of eddy fields in the northern North Atlantic as deduced from satellite-tracked buoys. *J. Mar. Res.*, **45**, 259–291, doi:[10.1357/00224087788401142](https://doi.org/10.1357/00224087788401142).
- LaCasce, J. H., 2008: Statistics from Lagrangian observations. *Prog. Oceanogr.*, **77**, 1–29, doi:[10.1016/j.pocean.2008.02.002](https://doi.org/10.1016/j.pocean.2008.02.002).
- Lumpkin, R., 2003: Decomposition of surface drifter observations in the Atlantic Ocean. *Geophys. Res. Lett.*, **30**, 1753, doi:[10.1029/2003GL017519](https://doi.org/10.1029/2003GL017519).
- , and M. Pazos, 2007: Measuring surface currents with surface velocity program drifters: The instrument, its data, and some recent results. *Lagrangian Analysis and Prediction of Coastal and Ocean Dynamics*, A. Griffa et al., Eds., Cambridge University Press, 39–67.
- , and G. C. Johnson, 2013: Global ocean surface velocities from drifters: Mean, variance, El-Niño Southern Oscillation response, and seasonal cycle. *J. Geophys. Res. Oceans*, **118**, 2992–3006, doi:[10.1002/jgrc.20210](https://doi.org/10.1002/jgrc.20210).
- , A.-M. Treguier, and K. Speer, 2002: Lagrangian eddy scales in the northern Atlantic Ocean. *J. Phys. Oceanogr.*, **32**, 2425–2440, doi:[10.1175/1520-0485-32.9.2425](https://doi.org/10.1175/1520-0485-32.9.2425).
- , S. A. Grodsky, L. R. Centurioni, M.-H. Rio, J. A. Carton, and D.-K. Lee, 2013: Removing spurious low-frequency variability in drifter velocities. *J. Atmos. Oceanic Technol.*, **30**, 353–360, doi:[10.1175/JTECH-D-12-00139.1](https://doi.org/10.1175/JTECH-D-12-00139.1).
- Maurizi, A., A. Griffa, P.-M. Poulaing, and F. Tampieri, 2004: Lagrangian turbulence in the Adriatic Sea as computed from drifter data: Effects of inhomogeneity and nonstationarity. *J. Geophys. Res.*, **109**, C04010, doi:[10.1029/2003JC002119](https://doi.org/10.1029/2003JC002119).
- McClean, J. L., P.-M. Poulaing, J. W. Pelton, and M. E. Maltrud, 2002: Eulerian and Lagrangian statistics from surface drifters and a high-resolution POP simulation in the North Atlantic. *J. Phys. Oceanogr.*, **32**, 2472–2491, doi:[10.1175/1520-0485-32.9.2472](https://doi.org/10.1175/1520-0485-32.9.2472).
- Niiler, P. P., 2001: The world ocean surface circulation. *Ocean Circulation and Climate: Observing and Modelling the Global Ocean*, G. Siedler et al., Eds., Academic Press, 193–204.
- Oh, I. S., V. Zhurbas, and W. Park, 2000: Estimating horizontal diffusivity in the East Sea (Sea of Japan) and the northwest Pacific from satellite-tracked drifter data. *J. Geophys. Res.*, **105**, 6483–6492, doi:[10.1029/2000JC900002](https://doi.org/10.1029/2000JC900002).
- Poulaing, P.-M., 2001: Adriatic Sea surface circulation as derived from drifter data between 1990 and 1999. *J. Mar. Syst.*, **29**, 3–32, doi:[10.1016/S0924-7963\(01\)00007-0](https://doi.org/10.1016/S0924-7963(01)00007-0).
- , and E. Zambianchi, 2007: Surface circulation in the central Mediterranean Sea as deduced from Lagrangian drifters in the 1990s. *Cont. Shelf Res.*, **27**, 981–1001, doi:[10.1016/j.csr.2007.01.005](https://doi.org/10.1016/j.csr.2007.01.005).
- , R. Gerin, E. Mauri, and R. Pennel, 2009: Wind effects on drogued and undrogued drifters in the eastern Mediterranean. *J. Atmos. Oceanic Technol.*, **26**, 1144–1156, doi:[10.1175/2008JTECHO618.1](https://doi.org/10.1175/2008JTECHO618.1).
- Qian, Y.-K., S. Peng, and Y. Li, 2013: Eulerian and Lagrangian statistics in the South China Sea as deduced from surface drifters. *J. Phys. Oceanogr.*, **43**, 726–743, doi:[10.1175/JPO-D-12-0170.1](https://doi.org/10.1175/JPO-D-12-0170.1).
- Rio, M.-H., 2012: Use of altimeter and wind data to detect the anomalous loss of SVP-type drifter's drogue. *J. Atmos. Oceanic Technol.*, **29**, 1663–1674, doi:[10.1175/JTECH-D-12-00008.1](https://doi.org/10.1175/JTECH-D-12-00008.1).
- Riskin, H., 1996: *The Fokker-Planck Equation: Methods of Solution and Applications*. 2nd ed. Springer-Verlag, 472 pp.
- Rupolo, V., 2007: A Lagrangian-based approach for determining trajectories taxonomy and turbulence regimes. *J. Phys. Oceanogr.*, **37**, 1584–1609, doi:[10.1175/JPO3038.1](https://doi.org/10.1175/JPO3038.1).
- Sallée, J. B., K. Speer, R. Morrow, and R. Lumpkin, 2008: An estimate of Lagrangian eddy statistics and diffusion in the mixed layer of the Southern Ocean. *J. Mar. Res.*, **66**, 441–463, doi:[10.1357/0022408787157458](https://doi.org/10.1357/0022408787157458).
- Shenoi, S. S. C., P. K. Saji, and A. M. Almeida, 1999: Near-surface circulation and kinetic energy in the tropical Indian Ocean derived from Lagrangian drifters. *J. Mar. Res.*, **57**, 885–907, doi:[10.1357/00224099321514088](https://doi.org/10.1357/00224099321514088).
- Sundermeyer, M. A., and J. F. Price, 1998: Lateral mixing and the North Atlantic Tracer Release Experiment: Observations and numerical simulations of Lagrangian particles and a passive tracer. *J. Geophys. Res.*, **103**, 21 481–21 497, doi:[10.1029/98JC01999](https://doi.org/10.1029/98JC01999).
- Swenson, M. S., and P. P. Niiler, 1996: Statistical analysis of the surface circulation of the California Current. *J. Geophys. Res.*, **101**, 22 631–22 645, doi:[10.1029/96JC02008](https://doi.org/10.1029/96JC02008).
- Taylor, G. I., 1922: Diffusion by continuous movements. *Proc. London Math. Soc.*, **20**, 196–212, doi:[10.1112/plms/s2-20.1.196](https://doi.org/10.1112/plms/s2-20.1.196).
- , 1953: Dispersion of soluble matter in solvent flowing slowly through a tube. *Proc. Roy. Soc. London*, **A219**, 186–203, doi:[10.1098/rspa.1953.0139](https://doi.org/10.1098/rspa.1953.0139).
- Thomson, D. J., 1987: Criteria for the selection of stochastic models of particle trajectories in turbulent flows. *J. Fluid Mech.*, **180**, 529–556, doi:[10.1017/S0022112087001940](https://doi.org/10.1017/S0022112087001940).
- Ursella, L., P.-M. Poulaing, and R. P. Signell, 2006: Surface drifter derived circulation in the northern and middle Adriatic Sea: Response to wind regime and season. *J. Geophys. Res.*, **111**, C03S04, doi:[10.1029/2005JC003177](https://doi.org/10.1029/2005JC003177).
- Veneziani, M., A. Griffa, A. M. Reynolds, and A. J. Mariano, 2004: Oceanic turbulence and stochastic models from subsurface Lagrangian data for the northwest Atlantic Ocean. *J. Phys. Oceanogr.*, **34**, 1884–1906, doi:[10.1175/1520-0485\(2004\)034<1884:OTASMF>2.0.CO;2](https://doi.org/10.1175/1520-0485(2004)034<1884:OTASMF>2.0.CO;2).
- , —, Z. D. Garraffo, and E. P. Chassignet, 2005: Lagrangian spin parameter and coherent structures from trajectories released in a high-resolution ocean model. *J. Mar. Res.*, **63**, 753–788, doi:[10.1357/002240054663187](https://doi.org/10.1357/002240054663187).
- Wunsch, C., 1996: *The Ocean Circulation Inverse Problem*. Cambridge University, 442 pp.
- Young, W. R., and S. Jones, 1991: Shear dispersion. *Phys. Fluids*, **3A**, 1087–1101, doi:[10.1063/1.858090](https://doi.org/10.1063/1.858090).
- Zhang, H.-M., M. D. Prater, and T. Rossby, 2001: Isopycnal Lagrangian statistics from the North Atlantic Current RAFOS float observations. *J. Geophys. Res.*, **106**, 13 817–13 836, doi:[10.1029/1999JC000101](https://doi.org/10.1029/1999JC000101).
- Zhurbas, V., D. Lyzhkov, and N. Kuzmina, 2014: Drifter-derived estimates of lateral eddy diffusivity in the world ocean with emphasis on the Indian Ocean and problems of parameterisation. *Deep-Sea Res. I*, **83**, 1–11, doi:[10.1016/j.dsr.2013.09.001](https://doi.org/10.1016/j.dsr.2013.09.001).